Tree-Inspired Lignin Microrods-Based Composite Heterogeneous Nanochannels for Ion Transport and Osmotic Energy Harvesting

Peng Cheng[a], Sheng Chen[a], Xin Li[a], Yanglei Xu[a, b, *, **], Feng Xu[a, **], Arthur J. Ragauskas[c, d]

[a]Beijing Key Laboratory of Lignocellulosic Chemistry, Beijing Forestry University, Beijing, 100083, P. R. China

[b]State Key Laboratory of Pulp and Paper Engineering, South China University of Technology, Guangzhou, 510640, P. R. China

[c]Department of Chemical and Biomolecular Engineering, University of Tennessee, Knoxville, TN 37996-2200, USA

[d]Joint Institute for Biological Sciences, Oak Ridge National Laboratory (ORNL), Oak Ridge, TN 37831, USA

*Corresponding authors: E-mail: xuyanglei@bjfu.edu.cn

**The two authors have the same contribution to this study.

Abstract:

One of the key processes of tree lignification is that lignin penetrates into the cell wall and fills in the cell wall framework, thereby increasing the hardness and hydrophobic of the tree channels, which is beneficial to consolidate and support the tree cell wall and water transport. Inspired by this natural process, we demonstrated a lignin-based nanofluidic heterogeneous membrane that closely mimics the channels in tree, which can realize ion transport function and effectively capture reverse electrodialysis. The membrane was synthesized by heating dealkaline lignin and PVA at 200°C and this formed fusiform microrods and a closed-packed membrane. Simultaneously, this membrane composited with anodized aluminum (AAO) channels membrane at 200°C to form asymmetric heterogeneous nanochannels membrane, which can transport counter-ions and harvest osmotic energy. This membrane implements ion current rectification in 0.1 M KCl electrolyte solution at pH 3 due to the confinement of pores and opposite surface charges in lignin-based heterogeneous nanochannel. An output power density of 0.97 W m^{-2} is obtained under a 50-fold salinity gradient, which can be further improved to 1.19 W m^{-2} by increasing the salinity gradient from 50-fold to 500-fold. Accordingly, this nanofluidic membranes were prepared by using lignin, the key component in tree, which not only mimicked a crucial process of the water and ionic transport process of channels in tree, but also had the prospect in the field of osmotic energy harvesting.

Keywords: Biomimetic; Lignin; Heterogeneous nanochannels; Ion Transport; Osmotic Energy

Harvesting

1. Introduction

Plenty of functional channel structures exists in nature, which can efficiently generate and accumulate energy from the environment [1-4]. Ion channels have attracted much attention due to their delicate controllability of ion transport in biology. The size and charge selectivity of protein channels have been a focal point ever since Erwin Neher and Bert Sakmann were awarded the Nobel Prize in Physiology in 1991 for discovering intracellular ion channels and pioneering patch clamp technology [5]. The characteristic of channels formed during a long evolution process in the biological world is unique [6]. The preparation of biomimetic lignin channel materials and devices strive to obtain a bioinspired ion channel structure, which provides a research basis for ion transportation and energy conversion [7,8].

Inspired by the precise control of ion transmembrane through ion channels on the cell membrane of being life, a series of preliminary studies on biomimetic artificial nanopores have been initiated, realizing the intelligence controllability of ion flux that originate from nanoconfinement [9-14]. The viewpoint that the single structural composition of the homogeneous nanoporous system limits its accurate controllability for ion transportation properties has been proposed [15-17]. Compared with the homogeneous nanoporous system, the multi-level pore structures composite of heterogeneous membrane system has the characteristics of more accurate controllability such as ionic diode effect due to asymmetric flow of ionic species caused by the synergistic effect between the two layers with inherent asymmetric structure and charge [16,18]. Therefore, it is imperative to construct multi-level pore structures in the homogeneous membrane and to develop a high-stability multifunctional composite heterogeneous membrane system for ion transport.

In competition for sunlight, trees evolved structural feature to defy gravity [19,20], as shown in Fig. 1a. The xylem of trees (a structure responsible for transporting water and minerals) contains a large amount of lignin, which contains multi-channels structure. The channels reinforced by lignin can resist the pressure generated by water in the cellular wall due to water transportation in transpiration, so as not to cause cell deformation or disruption. In this work, lignin strengthened a heterogeneous composite membrane to resist membrane deforming during ion transportation. Lignin materials exhibit surface negative charge due to their amorphous polymer structure consisting of aromatic alcohols [21-23]. So lignin-based composite membrane owns the ability of transporting counter-ions in the confined nanochannels. The hydrophobicity of lignin is another major characteristic, which can give tree high chemical stability in water [24-28] and benefit to ion transportation. The fabrication of tree-inspired energy conversion systems with good material strength, hydrophobicity, negative charge characteristics, nanostructure, superior underwater chemical stability and surface composition controllability has become the direction of continuous improvement in this developing field [29,30], which is further used as the basis of the application in the field of osmotic energy harvesting. Lignin materials are well match the for the above properties, their application in energy products (lignin-based salt difference power generation membrane) [31-33] will provide a new technical route for the development of value-added materials for the biomass industry [34].

In this work, we demonstrated a lignin microrods/ anodic aluminum oxide (AAO) (hereinafter "lignin/AAO") heterogeneous nanochannels membrane, which as consistent with the xylem of trees, containing a large amount of lignin and vesicular structures responsible for transporting water and minerals as shown in Fig. 1b and 1c. Lignin facilitated trees the capability to build upward, as shown in Fig. 1a. Numerous vesicular structures supported by lignin in xylem as channels for the exchange of water and substances between cells. Similarly, we developed artificial ion channels that utilize the compounds of fusiform lignin microrods (Fig. 1d) and polyvinyl alcohol (PVA) covered on the surface and wall of the AAO channels to form the heterogeneous nanochannels. As illustrated in Fig. 1e, with the synergism between the heterostructures and the peculiar nano-environment of the negatively charged surface, artificial nanochannel systems can rectify the ionic current and preserves charge-governed ionic transport in different electrolyte solutions. The membrane system generates electrical energy by mixing artificial seawater and river water due to reverse electrodialysis, as expected.

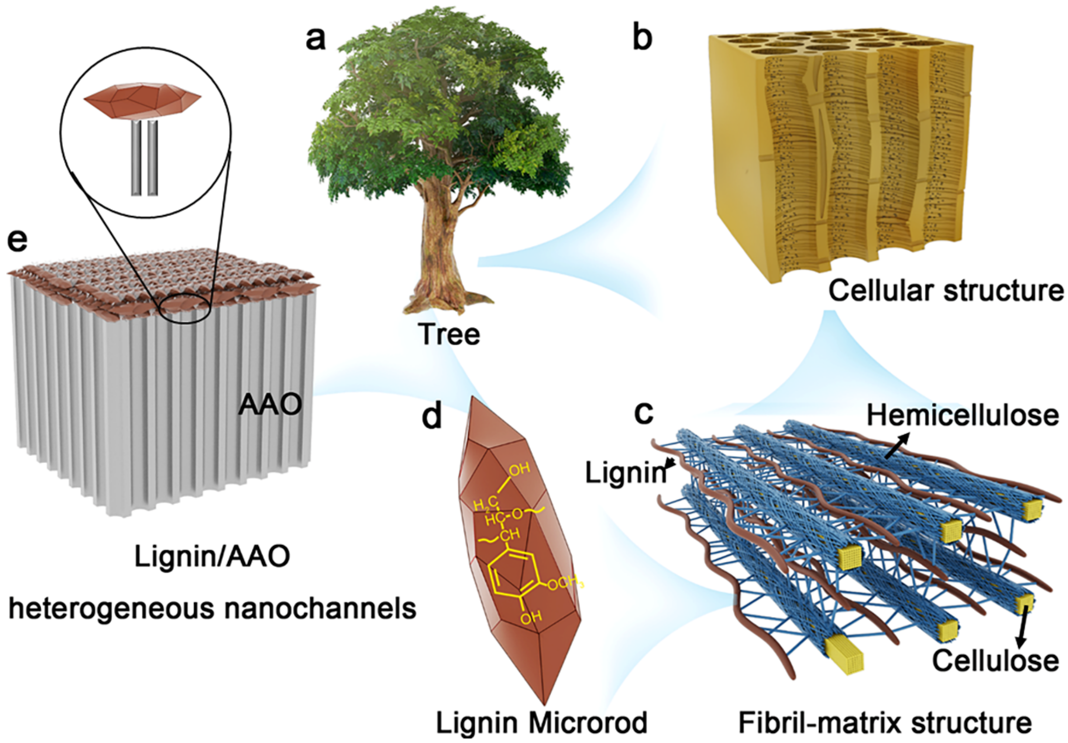

Fig. 1. The scheme of tree-inspired channels. (a) A tree. (b) Cellular structure. The xylem of trees contained a large amount of lignin and vesicular structures responsible for transporting water and minerals. (c) Fibril-matrix structure. The ultrastructure of tree cell walls including lignin, cellulose and hemicellulose. (d) The fusiform lignin microrods. (e) The lignin/AAO heterogeneous nanochannels membrane is consistent with the xylem of trees.

2. Experimental section

2.1 Materials

Dealkaline lignin (M_W 418.53 g/mol) and polyvinyl alcohol (alcoholysis degree 1788) were purchased from Shanghai Mclean Biochemical Technology Co., Ltd. The AAO membrane (40-70 nm pore size and diameter of 12 mm) was purchased from Hefei Pu-Yuan Nano Technology. All chemicals were used as received.

2.2 Preparation of PVA solution

0.54 g polyvinyl alcohol was dissolved in 10 mL deionized water (DI)/ethanol (50/50 Vol%) mixture at 80 °C [35].

2.3 Synthesis of heterostructure membrane

0.225 g, 0.45 g and 0.90 g dealkaline lignin were dispersed in 2 mL PVA solution by mechanical stirring and ultrasonic for 4 h and 15 min, respectively. The three kinds of lignin addition ways were labelled as L-0.225, L-0.45 and L-0.9. Then the mixed solution was spread uniformly onto the AAO membrane by glass rod wrapped with 1mm-thickness tape on both sides. Finally, the lignin /AAO heterostructure membrane was obtained after heat treatment at 200 °C for 40 min [35]. All the lignin /AAO membranes mentioned in this paper refer to the membranes prepared by the lignin addition ways of L-0.45 unless otherwise specified.

2.4 Characterization

Scanning electron microscope (SEM) was performed using a Hitachi SU-8010 instrument with the acceleration voltage of 5 kV. Fourier transform infrared spectroscopy was carried out using a ERTEX70. Spectra were obtained using an average of 16 scans with a resolution of 2 cm^{-1}. Contact angle measurements were measured at a Kino SL200KS with deionized water. Thermogravimetric analysis (TGA) curves were achieved by a DTG-60 at a heating rate of 10 °C min^{-1} under an air atmosphere. X-ray photoelectron spectroscopy (XPS) spectra was collected on a Thermo Scientific K-Alpha instrument with monochromated Al Kα radiation (1486.6 eV) at 12 kV under a pressure of 3×10^{-7} mbar. Zeta potential of PVA/lignin membrane and AAO were measured using a Malvern Zetasizer Nano ZS90 and an Anton Paar Surpass 3, respectively.

2.5 Electrical measurements

The ionic transport properties and the energy conversion tests of this lignin/AAO heterostructure membrane were measured by a Keithley 6487 semiconductor picoammeter (Keithley Instruments, Cleveland, OH) using a pair of Ag/AgCl electrodes. The heterogeneous membrane was mounted in the middle of the testing chamber filled with electrolyte solutions. The anode was set on the AAO side without specific instructions. The effective test experimental area of this membrane was ~ 0.5 mm^2. All electrolyte solutions were prepared using Watsons water. The pH values of electrolyte solutions were adjusted using HCl and $C_4H_{11}NO_3$ solutions. Three electrical measurements were carried out under the same conditions. Error bars of *I–V* curves were given by the standard deviation of three measurements under the same conditions.

2.6 The electrochemical impendence

EIS measurements were carried out in different electrolyte solutions (0.1 M KCl, 0.1 M NaCl, 0.1 M LiCl, 0.1 M $MgCl_2$, 0.1 M $CaCl_2$ and 0.1 M $AlCl_3$) at room temperature using an Electrochemical working station (Autolab 302N, Switzerland). The lignin/AAO membrane was fixed between two testing chambers. Two platinum electrodes were installed in the two testing chambers and sustained at the same interval and depth. The impedance spectra were measured in the frequency range from 10000 to 0.01 Hz at AC amplitude of 0.05 V.

2.7 Numerical Simulation

The theoretical model was calculated and found by Poisson and Nernst-Planck (PNP) equations (COMSOL 5.4a).

3. Results and discussion

De-alkaline lignin, a hydrophobic dealkaline polymer, when combined with PVA can form a free-standing cross-linked membrane, which was tethered on the surface of AAO membrane with hydroxyl groups through high temperature heating at 200 °C to construct the bioimimetic hybrid nanochannel membrane in this work. (see Experimental section, and Fig. S1). An AAO membrane was adopted as the substrate for the coating of lignin membrane. PVA serves as a bridge connecting two lignin units as well as lignin with AAO. Fig. 2a shows the fabrication processes for the lignin/AAO heterogeneous nanochannels membrane (details in Experimental section). The schematic diagram for the lignin membrane, AAO nanochannels membrane and lignin/AAO heterogeneous nanochannels membrane is shown in Fig. 2. The assembled structure of the lignin/AAO heterogeneous membrane was imaged by scanning electron microscopy (SEM). Before heating, the length of lignin nanoparticles is 0.1~1 μm, the shape is near-spherical, as shown in Fig. 2b. The morphology of lignin changes from near-microspheres to microrod. Lignin microrods are connected to each other though PVA to form disordered close-packed microrods layers at 200 °C heating. The thermogravimetric analysis and derivative thermogravimetric analysis show the dehydration process of lignin and PVA from 0 °C to 600 °C in Fig. 2f and Fig. S2, respectively, which also affect the assembling process of lignin hybrid membrane [36,37]. As shown in Fig. 2c, the length of lignin microrods is 0.5~2 μm, and the width of lignin microrods is 0.1~0.5 μm. With the increase of temperature, the particle size grew larger, and the morphology is regular. The surface properties of lignin/AAO heterogeneous nanochannel membrane before and after heating processing were studied by contact angle (CA) measurements. As shown in Fig. S3, the test results show that the obvious changes of the surface wettability occurred. The water CA of the lignin membrane is ~66 ^{o}, and increases to ~96^{o} after heating processing that it is because of dehydration reactions occurring on the surface PVA surface after heated at 200°C.

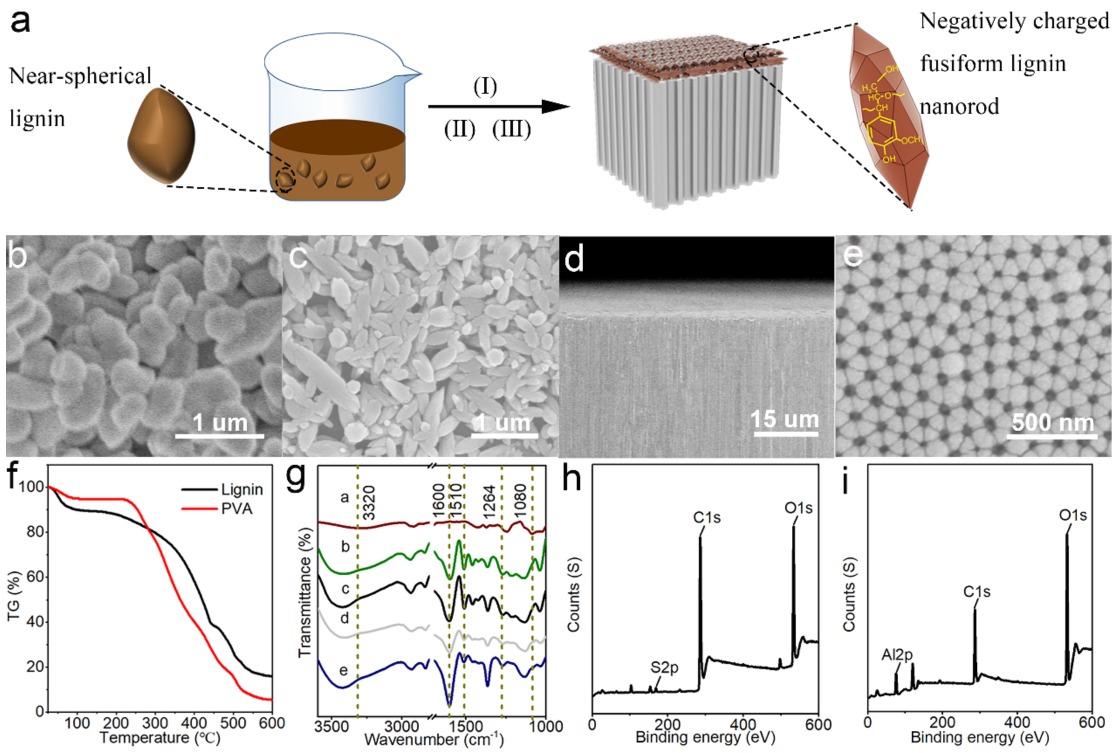

Fig. 2. The fabrication and characterization for the lignin /AAO heterogeneous nanochannels membrane. (a) The fabrication processes of the lignin /AAO heterogeneous nanochannels membrane. (I) Disperse the lignin in PVA solution. (II) Spread the above solution onto the AAO membrane. (III) Heat treatment to stabilize the lignin/AAO heterogeneous nanochannels membrane. (b) SEM photograph of diamond lignin nanoparticles. (c) SEM photograph of lignin membrane after 200°C heating. (d) The cross-section SEM photograph of lignin /AAO heterogeneous nanochannels membrane. (e) SEM photograph of AAO nanochannels. And the cross-section SEM photograph of AAO in the inset. (f) The thermogravimetric analysis of lignin and PVA from 25 °C to 600 °C. (g) The IR spectrum of PVA, lignin, and PVA/lignin before and after heating. (h) The XPS spectrum of lignin. (i) The XPS spectrum of AAO.

To further examine the structure of the lignin/AAO heterogeneous membrane, the cross-section SEM image reveals that the membrane has an ultrathin micron-scale thickness of approximately 90 μm (Fig. S4). Fig. 2d exhibits a 10 μm-thick PVA/lignin layers attaching onto an 80 μm-thick AAO nanochannels substrate membrane. The lignin close-packed layers covered and filled into the AAO nanochannels, which reduced the one side of pores size of AAO nanochannels to form asymmetric heterogeneous nanochannels (Fig. 2d). The pore diameter of AAO nanopores is ~40 nm, as shown in Fig. 2e. The cross-section SEM photograph of AAO shows in the inset of Fig. 2e. SEM data of the as-prepared lignin/AAO heterogeneous membrane is shown in Fig. S1. In the IR spectrum of Fig. 2g, the characteristic bands in the region 3320 cm^{-1} and 1080 cm^{-1} can be regarded as features of the hydroxy group in PVA [38]. Three characteristic peaks of lignin before (Line b) and after (line c) heating processing, 1600 cm^{-1}, 1510 cm^{-1}, and 1264 cm^{-1}, are observed [39]. Line d and e are the

IR spectrum of PVA/lignin membrane before and after heated treatment. As shown in Fig. 2g (line e), the 3320 cm^{-1}, 1600 cm^{-1}, 1510 cm^{-1}, 1264 cm^{-1} and 1080 cm^{-1} are characteristic peaks of lignin membrane, which proves that the lignin and PVA have been successfully mixed together. X-ray photoelectron spectroscopy (XPS) analysis was used to detect the content of carbon, oxygen and aluminum contained in lignin and AAO, respectively. As shown in Fig. 2h and 2i, the appearance of C_{1s}, O_{1s} signal in lignin and the appearance of Al_{2S} and O_{1s} signal in AAO can further illustrate the elementary composition.

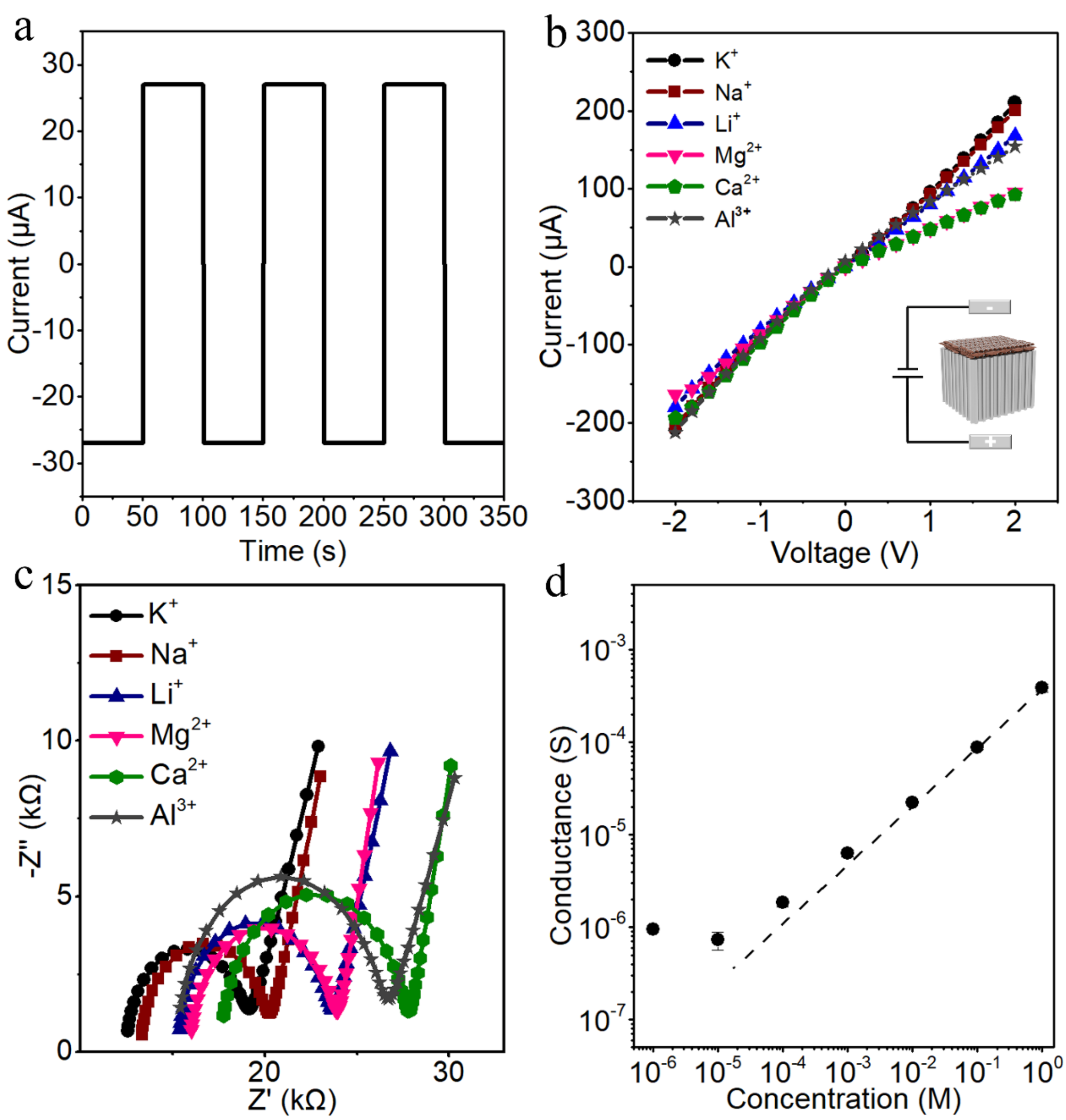

Fig. 3. The stability and ion transport properties of the lignin /AAO heterogeneous membrane. (a) The ionic current curve of the membrane with an alternately external bias of +2 V/-2 V shows its stable ion transport property. (b) Ionic current of the lignin /AAO membrane for different cations. (c) Nyquist curves of six cations (K^+, Na^+, Li^+, Mg^{2+}, Ca^{2+}, and Al^{3+}) at 25 °C. (d) Impact of the KCl concentration on ionic conductance.

Ion current is the main experimental observable that was recorded by the current-time *(I-T)* curve and the ionic current-transmembrane voltage *(I-V)* curve. The *I-T* curve of the lignin /AAO heterogeneous membrane is alternately applied with an external bias of +2 V/-2 V. Fig. 3a shows both negative and positive ionic currents are relatively constant, and each cycle can last for 50 s and repeat 7 times, indicating the excellent chemical stability of our lignin-based heterogeneous membrane system. The ionic transport property and ion selectivity of the lignin/AAO heterogeneous membrane were studied with an electrochemical system by measuring *I-V* curves. A pair of Ag/AgCl electrodes inserted into the reactive chamber on both sides of lignin /AAO membrane served as working electrode. The *I-V* characteristic curves of lignin/AAO heterogeneous membrane were studied through an external bias from -2 V to +2 V with different electrolyte solutions [40], as shown in Fig. 3b. The inset of Fig. 3b shows the direction of cationic flux and anionic flux at different bias. In the heterogeneous nanochannels system with 40 nm-pore AAO nanochannel, the *I-V* curve presents linear ohmic behavior with negligible ionic current rectifying phenomenon in 0.1 M KCl, 0.1 M NaCl and 0.1 M LiCl electrolyte solution at pH 7, which can be ascribed to the identical surface charges of the composite system. Notably, the system demonstrates ionic current rectification in 0.1 M $MgCl_2$ or 0.1 M $CaCl_2$ electrolyte solution at pH 7, arising from large hydrated ionic radius and intrinsic charge [41,42].

To further study the different cations transmembrane property, the ac impedance spectra of the lignin-based heterogeneous membrane in $AlCl_3$, $MgCl_2$, $CaCl_2$, LiCl, NaCl and KCl electrolyte solutions (0.1 M) were tested. The two platinum plates were used as working electrode and assistant electrodes, respectively [43]. Fig. S5 shows the equivalent circuit (some details in supporting information). Fig. 3c shows impedance Nyquist curve in Al^{3+}, Mg^{2+}, Ca^{2+}, Li^{+}, Na^{+} and K^{+}. According to the equivalent circuit, the membrane resistance (Rm), solution resistance (Rs) and charge transfer resistance (Rcf) were calculated and shown in Table. S1. For the monovalent ions, Rm of K^{+} is the smallest due to the low charge and relatively larger diffusion coefficient (1.960×10^{-9} m^2 s^{-1}), and the value of Rm is 6548.8 Ω. The faster the cation transport, the smaller Rm is, which is a typical cation-selective membrane. Despite the diffusion coefficient of Mg^{2+} (0.705×10^{-9} m^2 s^{-1}) is lower than that of Li^{+} (1.03×10^{-9} m^2 s^{-1}), the calculated Rm of Li^{+} is much larger that of Mg^{2+}, which was attributed to the stronger electrostatic interaction of large intrinsic charge [17,44,45] (Some detailed including equivalent circuit in supporting information).

In the heterogeneous nanochannels system with a 20 nm-pore AAO nanochannel, the *I-V* curve is also linear straight line at pH 7 and 10 (Fig. 4a). The *I-V* curve presents ion current rectification in 0.1 M KCl electrolyte solution at pH 3 due to the confinement of pores and opposite surface charges in lignin-based heterogeneous nanochannel. The inner walls of the AAO nanochannels carry hydroxyl groups and its isoelectric point is ca. 5.31, which was confirmed by zeta-potential measurements. The hybrid membrane is filled with lignin containing aliphatic hydroxyl groups and phenolic hydroxyl groups, where zeta potential is more negative. The zeta potential results suggest surface charges difference characteristic in the lignin membrane and AAO membrane when exposed to different pH (Fig. 4b). At pH is 4, the zeta potential of lignin membrane is -44 mV, and that of AAO membrane is 15 mV, resulting in the obvious opposite surface charges. As shown in Fig. 3d, surface charges mainly govern the ion transport property in diluted electrolyte, and bulk concentration takes charge of ion transport property in a higher concentration electrolyte, which is consistent with our previous reported papers [46].

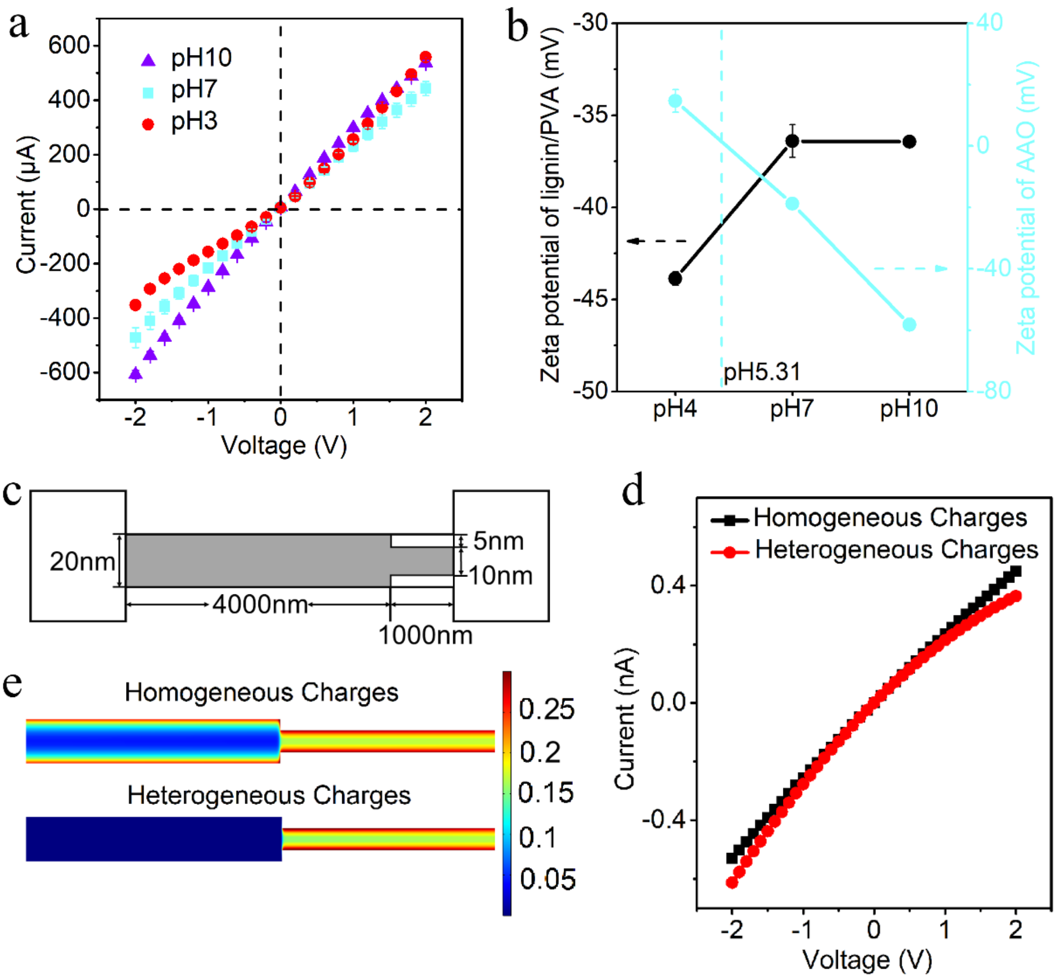

Fig. 4. Ion transport properties and numerical simulation of heterogeneous nanochannels with asymmetric pore. (a) *I*−*V* curves of the lignin/AAO membrane with the AAO channel size of 20 nm in 0.1 M KCl solution under different pH values. (b) The zeta potential of lignin/PVA membrane and AAO, respectively. (c) The schematic of nanochannel model. The total length of nanochannel is 5000 nm, that of lignin channels is 1000 nm, and that of AAO channels is 4000 nm. The size of AAO nanochannel diameter of model is ~20 nm. The size of PVA/lignin hybrid pore is ~10 nm, and its pore distance is ~10 nm. (d) The simulated *I-V* curves of nanochannels with homogeneous charges and heterogeneous charges. (e) The calculated profile inside the nanochannels with homogeneous charges and heterogeneous charges.

The rectification property of diodes composed of lignin (surface carry aliphatic hydroxyl groups and phenolic hydroxyl groups) and AAO (hydroxyl groups, Isoelectric point ≈ 5.31) at pH 3 and pH 10 under the external electric field was calculated using Poisson-Nernst-Planck equations based on a theoretical model [47]. According to the surface charges and structure characteristics of heterogeneous membrane, the heterogeneous lignin channel and AAO channel are approximate to an asymmetric nanochannel in the simulated model. The schematic of the simulated model is shown in Fig. 4c. The pore diameter lignin channel was set as 10 nm, that of AAO channel is 20 nm. The charge densities of PVA/lignin hybrid channel and AAO channel were set to be -0.0002 mC m^{-2}, +0.0002 mC m^{-2} at pH 3, while these were set to be -0.0002 mC m^{-2}, -0.0002 mC m^{-2} at pH 10. Other boundary conditions in detail are explained in Note. S1. Fig. 4d shows the *I-V* curve simulated by PNP model when the heterogeneous membrane system was set as pH 10. The rectification ratio is 1.18. When pH decreases from 10 to 3, the *I-V* curve shows higher ion current rectification, arising from the heterogeneous surface charges of lignin and AAO nanochannels at pH 3. According to the *I-V* curves in Fig. 4d, the ion rectification ratio can be calculated as 1.69, which accords with the experimental results in Fig. 4a. Fig. 4e shows the cations accumulated on the whole nanochannel at pH 3 because of homogeneous charges on the internal surface of nanochannel. In general, both anions and cations are accumulated on the lignin/AAO nanochannels, respectively. The simulated results display ion current rectification property, which keep constant with experimental results. Our theoretical results verify that asymmetric nanochannel with heterogeneous charges brings a higher ion current rectification ratio and reveal that the ion current rectification stems from the ion concentration enrichment and depletion.

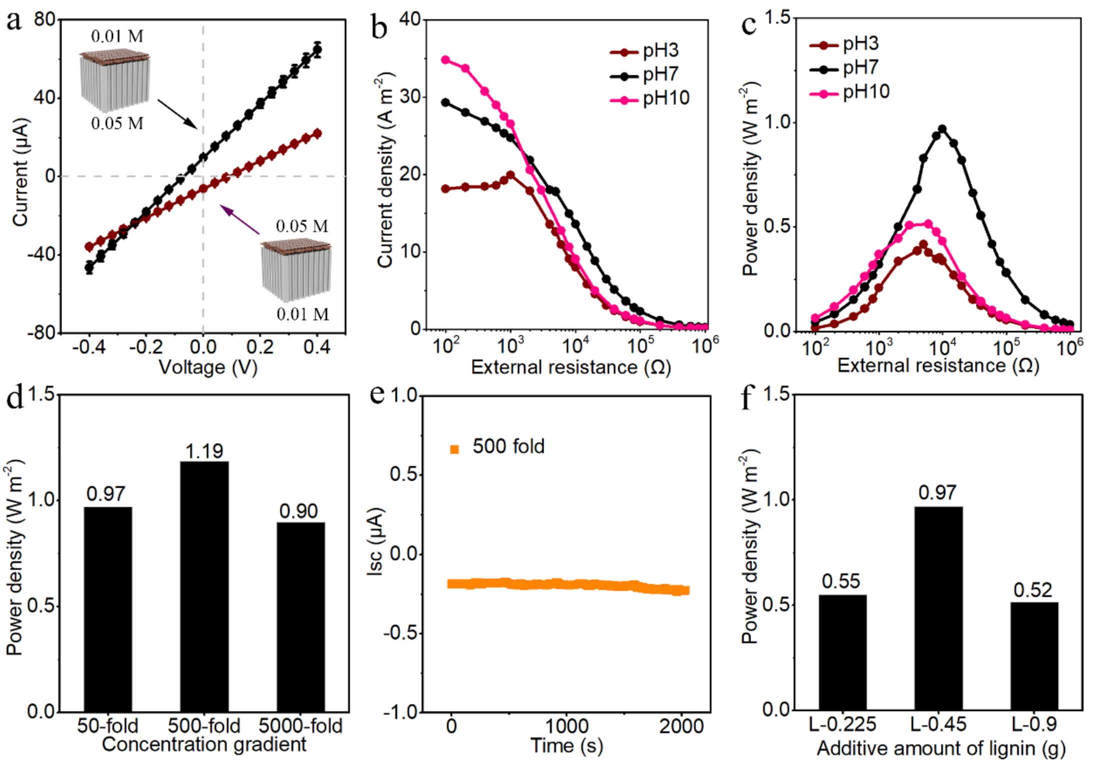

Fig. 5. Application for harvesting osmotic energy. (a) *I-V* curves of the lignin /AAO membrane under two configured NaCl concentration gradients. (b) The current density of the membrane in 0.5 M/0.01 M NaCl solution at different pH values. (c) The effect of external resistance on the power density. (d) The power density at different salinity gradients under pH 7. (e) The output diffusion current at a 500-fold salinity gradient under pH 7. (f) The output power density of the membranes with different additive amount of lignin (Labelled as L-0.225, L-0.45 and L-0.9) at a 50-fold salinity gradient.

To study ion selectivity of heterogeneous membrane, the transmembrane current among salinity gradients solution presented in this work were performed with the *I-V* curves. As illustrated in the inset of Fig. 5a, anode and cathode were placed in the concentrated concentration electrolyte and diluted concentration electrolyte, respectively. Cations diffusion along salinity gradient could produce a forward current due to continuous diffusion, whereas anions diffusion could generate a backward one due to electrostatic force, which results in a positive net cation transmembrane current. Fig. 5a shows the *I-V* curve deviates to positive current without passing zero. When the salinity gradient was reversed, the *I-V* curve shifted in a negative current direction, suggesting a net cation current formation. Under two cases of reverse salinity gradient, the I_{diff} and V_{diff} show non-uniform values due to the different cation diffusion phenomena, resulting in an opposite polarity direction. Their phenomena suggest that the heterogeneous membrane prefers ion diffusion direction from lignin to AAO channels.

To further investigate the effect of surface charge on output power harvesting, the electroosmotic behaviors at different pH were explored. This power output density can be obtained through the equation $P = I_d^2 \times R_L/S$, where I_d is the diffusion current, S is active area, R_L is a load resistor in an external circuit, and can be adjusted the range from 100 Ω to 10^6 Ω. Fig. 5b shows different current densities change with the increase of load resistor under different pH values. A significant increase in output power density (0.97 W m^{-2}) is obtained under middle pH at 50-fold salinity gradient in Fig. 5c due to the enriched surface charges of channel, suggesting that the surface charges property and pore structure of nanochannels serve as key roles in osmotic power harvesting. And the energy conversion efficiency is approximately 34.1%. Some details of the calculated equation are shown in Note. S2. The value of output power density is higher than that those of most of the previously reported homogeneous and heterogeneous nanofluidic membrane based the reverse electrodialysis technology, such as CNM [48], bacterial cellulose pair [49], PET [46], ABN [50], GOM [51], TOCN/PET [46] and MMT [52] under 50-fold salinity gradient (Fig. S6). Although the value is still lower than that of the existed CMN/AAO [53], ionomer/AAO [54] and polyelectrolyte hydrogel/ANF [55] membranes, these heterogeneous nano materials is expensive, complex and time-consuming to prepare, making large-scale fabrication difficult. Lignin widely exists in trees and other plant raw materials, and can be easily obtained in the form of by-products of papermaking industry. Lignin-based membrane using in nanofluidic system has the advantages of low cost, simple preparation and large-scale application. The osmotic power harvesting was evaluated by recording the *I-V* curves under different salinity gradients from 50-fold to 5000-fold at pH 7. Their maximum values of output power density can be calculated and achieves of 1.19 W m^{-2} at the load resistance of 12 kΩ at 500-fold (Fig. 5d). That's because ion concentration polarization effect at the surface of heterogeneous membranes enhances when the salinity gradient increases. The output diffusion current under a 500-fold salinity gradient was investigated (Fig. 5e). For the heterogeneous membrane, the output current can keep a stable value, suggesting outstanding stability. Fig. 5f shows output power density of the membranes with different additive amount of lignin. The maximum power density is lignin/AAO membrane with L-0.45, which can be ascribed to the enriched surface charges density. Decreasing additive amount to L-0.225, the power density reduces to 0.55 W m^{-2} due to the sparse surface charges densities. Increasing additive amount to L-0.9 induce a decrease of power density to 0.52 W m^{-2}. The excess lignin will introduce an increase of slits between lignin and PVA, resulting in a decreased power density. The ionic current, diffusion current and power density of the membranes with different additive amount of lignin are listed in Table S2. Overall, the lignin-based heterogeneous membrane shows high-performance osmotic energy conversion.

4. Conclusions

In conclusion, we report a tree-inspired green renewable lignin-based heterogeneous nanochannels membrane. The current rectification is induced directly by the protonation of surface charges due to the pH change of electrolyte solutions. For simulation, the results employed by PNP model coincide with the experimental results. The effect of surface charges of the channels on the osmotic energy harvesting has been investigated. The implementation of artificial seawater and river water on the lignin/AAO heterogeneous nanochannels membrane can deliver an output power density of 0.97 W m^{-2}. The construction of membrane served as a separator has become one of the most urgent research topics in fields related to osmotic energy harvesting. Therefore, we believe these results not only mimic a key step of water transport in tree growth, but also can help understand the impact of the lignin on surface negative charges, hydrophobicity of tree and anticipate wide potentials for osmotic energy harvesting. Although the lignin-based heterogeneous nanochannels membrane has good prospect for ionic transportation and osmotic energy harvesting, there are still some challenges to be worked out. There are no other studies on lignin-based nanochannel membranes and the output power density still falls short of commercial requirements. Additionally, the lignin has a poor characteristic of film formation. Future works will focus on increasing the power density of the lignin-based nanochannel membrane through the following three aspects: (1) More investigations should be performed for lignin-based nanochannel membrane. (2) Regulating the charge density, hydrophilicity and channel structure of lignin-based membrane by modifying lignin. (3) Fabricating thinner composite films to reduce the film resistance by selecting substrate materials with smaller thickness than AAO. In this way, with the progress of research and technology, it is expected to achieve better performance in the future.

CRediT authorship contribution statement

Peng Cheng: Methodology, Investigation, Formal analysis, Visualization, Writing –original draft. **Sheng Chen:** Methodology, Formal analysis. **Xin Li:** Software, Formal analysis. **Yanglei Xu:** Conceptualization, Resources, Data curation, Visualization, Formal analysis, Writing – original draft, Supervision, Funding acquisition. **Feng Xu:** Conceptualization, Writing – review & editing, Supervision, Funding acquisition. **Arthur J. Ragauskas:** Conceptualization. *Corresponding authors: Y. L. Xu and F. Xu have the same contribution to this study.

Declaration of Competing Interest

The authors declare that they have no known competing financial interests or personal relationships that could have appeared to influence the work reported in this paper.

Acknowledgements

This work is supported by the National Natural Science Foundation of China (Grant No. 21701159), the National Key R&D Program of China (2021YFC21013004), the Fundamental Research Funds for the Central Universities (BLX201916, PTYX202141), Programme of Introducing Talents of Discipline to Universities (Project 111, B21022) and State Key Laboratory of Pulp and Paper Engineering (Project No. 202101).

References

[1] Negi J, Matsuda O, Nagasawa T, Oba Y, Takahashi H, Kawai-Yamada M et al. CO_2 regulator slac1 and its homologues are essential for anion homeostasis in plant cells. Nature 2008; 452(7186): 483-486. https://doi:10.1038/nature06720.

[2] Frommer WB. Biochemistry. CO_2mmon sense. Science 2010; 327(5963): 275-276. https://doi:10.1126/science.1186022.

[3] Hinds BJ. Engineering small-ion transporter channels. Science 2021; 372(6541): 459-460. https://doi:10.1126/science.abh2618.

[4] Caterina MJ, Schumacher MA, Tominaga M, Rosen TA, Levine JD & Julius D. The capsaicin receptor: A heat-activated ion channel in the pain pathway. Nature 1997; 389(6653): 816-824. https://doi:10.1038/39807.

[5] Hamill OP, Marty A, Neher E, Sakmann B & Sigworth FJ. Improved patch-clamp techniques for high-resolution current recording from cells and cell-free membrane patches. Pflugers Archiv : European journal of physiology 1981; 391(2): 85-100. https://doi:10.1007/bf00656997.

[6] Mayer ML. Glutamate receptors at atomic resolution. Nature 2006; 440(7083): 456-462. https://doi:10.1038/nature04709.

[7] Siria A, Poncharal P, Biance AL, Fulcrand R, Blase X, Purcell ST et al. Giant osmotic energy

conversion measured in a single transmembrane boron nitride nanotube. Nature 2013; 494(7438): 455-458. https://doi:10.1038/nature11876.

[8] Tang CG, Ang MC, Choo KK, Keerthi V, Tan JK, Syafiqah MN et al. Doped polymer semiconductors with ultrahigh and ultralow work functions for ohmic contacts. Nature 2016; 539(7630): 536-540. https://doi:10.1038/nature20133.

[9] Liu Q, Tang ZT, Qu ZG, Ren QL, Zhang JF, Tang RX. A capacitor-based power equivalent model for salinity-gradient osmotic energy conversion. Energy Conversion and Management 250 (2021) 114862. https://doi.org/10.1016/j.enconman.2021.114862.

[10] Uliana AA, Bui NT, Kamcev J, Taylor MK, Urban JJ & Long JR. Ion-capture electrodialysis using multifunctional adsorptive membranes. Science 2021; 372(6539): 296-299. https://doi:10.1126/science.abf5991.

[11] Hummer G, Rasaiah JC & Noworyta JP. Water conduction through the hydrophobic channel of a carbon nanotube. Nature 2001; 414(6860): 188-190. https://doi:10.1038/35102535.

[12] Lu J, Zhang H, Hou J, Li X, Hu X, Hu Y et al. Efficient metal ion sieving in rectifying subnanochannels enabled by metal-organic frameworks. Nat Mater 2020; 19(7): 767-774. https://doi:10.1038/s41563-020-0634-7.

[13] Schmidt-Rohr K & Chen Q. Parallel cylindrical water nanochannels in nafion fuel-cell membranes. Nat Mater 2008; 7(1): 75-83. https://doi:10.1038/nmat2074.

[14] Li HZ, Qiu CL, Ren SJ, Dong QB, Zhang SX, Zhou FL et al. Na^+-gated water-conducting nanochannels for boosting CO_2 conversion to liquid fuels. Science 2020; 367(6478): 667-671. https://doi:10.1126/science.aaz6053.

[15] Xin W, Zhang Z, Huang X, Hu Y, Zhou T, Zhu C et al. High-performance silk-based hybrid membranes employed for osmotic energy conversion. Nat Commun 2019; 10(1): 3876. https://doi:10.1038/s41467-019-11792-8.

[16] Huang X, Kong X-Y, Wen L & Jiang L. Bioinspired ionic diodes: From unipolar to bipolar. Advanced Functional Materials 2018; 28(49): 1801079. https://doi:10.1002/adfm.201801079.

[17] Zhang Z, He L, Zhu C, Qian Y, Wen L & Jiang L. Improved osmotic energy conversion in heterogeneous membrane boosted by three-dimensional hydrogel interface. Nat Commun 2020; 11(1): 875. https://doi:10.1038/s41467-020-14674-6.

[18] Sun Y, Chen S, Chen X, Xu Y, Zhang S, Ouyang Q et al. A highly selective and recyclable no-

responsive nanochannel based on a spiroring opening-closing reaction strategy. Nat Commun 2019; 10(1): 1323. https://doi:10.1038/s41467-019-09163-4.

[19] Tester M & Davenport R. Na^+ tolerance and Na^+ transport in higher plants. Ann Bot 2003; 91(5): 503-527. https://doi:10.1093/aob/mcg058.

[20] Koch GW, Sillett SC, Jennings GM & Davis SD. The limits to tree height. Nature 2004; 428(6985): 851-854. https://doi:10.1038/nature02417.

[21] Scholander PF, Bradstreet ED, Hemmingsen EA & Hammel HT. Sap pressure in vascular plants: Negative hydrostatic pressure can be measured in plants. Science 1965; 148(3668): 339-346. https://doi:10.1126/science.148.3668.339.

[22] Kubo M, Udagawa M, Nishikubo N, Horiguchi G, Yamaguchi M, Ito J et al. Transcription switches for protoxylem and metaxylem vessel formation. Genes Dev 2005; 19(16): 1855-1860. https://doi:10.1101/gad.1331305.

[23] Gaymard F, Pilot G, Lacombe B, Bouchez D, Bruneau D, Boucherez J et al. Identification and disruption of a plant shaker-like outward channel involved in K^+ release into the xylem sap. Cell 1998; 94(5): 647-655. https://doi:10.1016/s0092-8674(00)81606-2.

[24] Kang X, Kirui A, Dickwella Widanage MC, Mentink-Vigier F, Cosgrove DJ & Wang T. Lignin-polysaccharide interactions in plant secondary cell walls revealed by solid-state NMR. Nat Commun 2019; 10(1): 347. https://doi:10.1038/s41467-018-08252-0.

[25] Liao YH, Koelewijn SF, Van den Bossche G, Van Aelst J, Van den Bosch S, Renders T et al. A sustainable wood biorefinery for low-carbon footprint chemicals production. Science 2020; 367(6484): 1385-1390. https://doi:10.1126/science.aau1567.

[26] Nakakuni M, Watanabe K, Kaminaka K, Mizuno Y, Takehara K, Kuwae T et al. Seagrass contributes substantially to the sedimentary lignin pool in an estuarine seagrass meadow. Sci Total Environ 2021; 793: 148488. https://doi:10.1016/j.scitotenv.2021.148488.

[27] Yang B, Ljung K, Nielsen AB, Fahlgren E & Hammarlund D. Impacts of long-term land use on terrestrial organic matter input to lakes based on lignin phenols in sediment records from a swedish forest lake. Sci Total Environ 2021; 774: 145517. https://doi:10.1016/j.scitotenv.2021.145517.

[28] Zhao B, Yao P, Li D & Yu Z. Effects of river damming and delta erosion on organic carbon burial in the changjiang estuary and adjacent east china sea inner shelf. Sci Total Environ 2021;

793: 148610. https://doi:10.1016/j.scitotenv.2021.148610.

[29] Xie M, Zhang J, Tschaplinski TJ, Tuskan GA, Chen JG & Muchero W. Regulation of lignin biosynthesis and its role in growth-defense tradeoffs. Front Plant Sci 2018; 9: 1427. https://doi:10.3389/fpls.2018.01427.

[30] Chezem WR, Memon A, Li FS, Weng JK & Clay NK. SG2-Type R2R3-MYB transcription factor MYB15 controls defense-induced lignification and basal immunity in Arabidopsis. Plant Cell 2017; 29(8): 1907-1926. https://doi:10.1105/tpc.16.00954.

[31] Rodriguez Couto S & Toca Herrera JL. Industrial and biotechnological applications of laccases: a review. Biotechnol Adv 2006; 24(5): 500-513. https://doi:10.1016/j.biotechadv.2006.04.003.

[32] Rahimi A, Ulbrich A, Coon JJ & Stahl SS. Formic-acid-induced depolymerization of oxidized lignin to aromatics. Nature 2014; 515(7526): 249-252. https://doi:10.1038/nature13867.

[33] Richter AP, Brown JS, Bharti B, Wang A, Gangwal S, Houck K et al. An environmentally benign antimicrobial nanoparticle based on a silver-infused lignin core. Nature Nanotechnology 2015; 10(9): 817-831. https://doi:10.1038/nnano.2015.141.

[34] Xia Q, Chen C, Yao Y, Li J, He S, Zhou Y et al. A strong, Biodegradable and recyclable lignocellulosic bioplastic. Nature Sustainability 2021; 4(7): 627-635. https://doi:10.1038/s41893-021-00702-w.

[35] Li R, Jiang J, Liu Q, Xie Z & Zhai J. Hybrid nanochannel membrane based on polymer/MOF for high-performance salinity gradient power generation. Nano Energy 2018; 53: 643-649. https://doi:10.1016/j.nanoen.2018.09.015.

[36] Song Y, Chandra RP, Zhang X & Saddler JN. Non-productive cellulase binding onto deep eutectic solvent (DES) extracted lignin from willow and corn stover with inhibitory effects on enzymatic hydrolysis of cellulose. Carbohydr Polym 2020; 250: 116956. https://doi:10.1016/j.carbpol.2020.116956.

[37] Guo Z, Zhang Q, You T, Zhang X, Xu F & Wu Y. Short-time deep eutectic solvent pretreatment for enhanced enzymatic saccharification and lignin valorization. Green Chemistry 2019; 21(11): 3099-3108. https://doi:10.1039/c9gc00704k.

[38] Zhang MK, Zhang XH & Han GZ. Magnetic alginate/PVA hydrogel microspheres with selective adsorption performance for aromatic compounds. Separation and Purification Technology 2022; 278: 119547. https://doi:10.1016/j.seppur.2021.119547.

[39] Li R, Wang XH, Lin QX, Yue FX, Liu CF, Wang XY et al. Structural features of lignin fractionated from industrial furfural residue using alkaline cooking technology and its antioxidant performance. Frontiers in Energy Research 2020; 8: 83. https://doi:10.3389/fenrg.2020.00083.

[40] Siwy ZS. Ion-current rectification in nanopores and nanotubes with broken symmetry. Advanced Functional Materials 2006; 16(6): 735-746. https://doi:10.1002/adfm.200500471.

[41] Zhang HC, Hou J, Hu YX, Wang PY, Ou RW, Jiang L et al. Ultrafast selective transport of alkali metal ions in metal organic frameworks with subnanometer pores. Science Advances 2018; 4(2): eaaq0066. https://doi:10.1126/sciadv.aaq0066.

[42] Sparreboom W, van den Berg A & Eijkel JC. Principles and applications of nanofluidic transport. Nat Nanotechnol 2009; 4(11): 713-720. https://doi:10.1038/nnano.2009.332.

[43] Yao L, Long Z, Chen Z, Cheng Q, Liao Y & Tian M. Property characterization and mechanism analysis of polyoxometalates-functionalized PVDF membranes by electrochemical impedance spectroscopy. Membranes 2020; 10(9): 214. https://doi:10.3390/membranes10090214.

[44] Lu B, Xiao T, Xu Y, Diao X & Zhai J. Kinetic process of an alkaline earth metal ion transmembrane through ZIF-8. J Phys Chem Lett 2021; 12(23): 5587-5592. https://doi:10.1021/acs.jpclett.1c01469.

[45] Freger V & Bason S. Characterization of ion transport in thin films using electrochemical impedance spectroscopy principles and theory. Journal of Membrane Science 2007; 302(1-2): 1-9. https://doi:10.1016/j.memsci.2007.06.046.

[46] Xu Y, Song Y & Xu F. Tempo oxidized cellulose nanofibers-based heterogenous membrane employed for concentration-gradient-driven energy harvesting. Nano Energy 2021; 79: 105468. https://doi:10.1016/j.nanoen.2020.105468.

[47] Constantin D & Siwy ZS. Poisson-Nernst-Planck model of ion current rectification through a nanofluidic diode. Phys Rev E Stat Nonlin Soft Matter Phys 2007; 76: 041202. https://doi:10.1103/PhysRevE.76.041202.

[48] Xiao K, Tu B, Chen L, Heil T, Wen L, Jiang L et al. Photo-driven ion transport for a photodetector based on an asymmetric carbon nitride nanotube membrane. Angewandte Chemie-International Edition 2019; 58(36): 12574-12579. https://doi:10.1002/anie.201907833.

[49] Wu Z, Ji P, Wang B, Sheng N, Zhang M, Chen S et al. Oppositely charged aligned bacterial cellulose biofilm with nanofluidic channels for osmotic energy harvesting. Nano Energy 2021; 80:

105554. https://doi:10.1016/j.nanoen.2020.105554.

[50] Chen C, Liu D, He L, Qin S, Wang J, Razal JM et al. Bio-inspired nanocomposite membranes for osmotic energy harvesting. Joule 2020; 4(1): 247-261. https://doi:10.1016/j.joule.2019.11.010.

[51] Ji J, Kang Q, Zhou Y, Feng Y, Chen X, Yuan J et al. Osmotic power generation with positively and negatively charged 2D nanofluidic membrane pairs. Advanced Functional Materials 2017; 27(2): 1603623. https://doi:10.1002/adfm.201603623.

[52] Wu C, Xiao T, Tang J, Zhang Q, Liu Z, Liu J et al. Biomimetic temperature-gated 2D cationic nanochannels for controllable osmotic power harvesting. Nano Energy 2020; 76: 105113. https://doi:10.1016/j.nanoen.2020.105113.

[53] Xie L, Zhou S, Liu J, Qiu B, Liu T, Liang Q et al. Sequential superassembly of nanofiber arrays to carbonaceous ordered mesoporous nanowires and their heterostructure membranes for osmotic energy conversion. J Am Chem Soc 2021; 143(18): 6922-6932. https://doi:10.1021/jacs.1c00547.

[54] Xiao T, Zhang Q, Jiang J, Ma J, Liu Q, Lu B et al. pH-resistant nanofluidic diode membrane for high-performance conversion of salinity gradient into electric energy. Energy Technology 2019; 7(5): 1800952. https://doi:10.1002/ente.201800952.

[55] Zhang Z, He L, Zhu C, Qian Y, Wen L & Jiang L. Improved osmotic energy conversion in heterogeneous membrane boosted by three-dimensional hydrogel interface. Nat Commun 2020; 11(1): 875. https://doi:10.1038/s41467-020-14674-6.